Gravity Currents from Instantaneous Sources Down a Slope

A. Dai[1]; C. E. Ozdemir[2]; M. I. Cantero[3]; and S. Balachandar[4]

Abstract: Gravity currents from instantaneous sources down a slope were modeled with classic thermal theory, which has formed the basis for many subsequent studies. Considering entrainment of ambient fluid and conservation of total buoyancy, thermal theory predicted the height, length, and velocity of the gravity current head. In this study, the problem with direct numerical simulations was re-investigated, and the results compared with thermal theory. The predictions based on thermal theory are shown to be appropriate only for the acceleration phase, not for the entire gravity current motion. In particular, for the current head forms on a 10° slope produced from an instantaneous buoyancy source, the contained buoyancy in the head is approximately 58% of the total buoyancy at most and is not conserved during the motion as assumed in thermal theory. In the deceleration phase, the height and aspect ratio of the head and the buoyancy contained within it may all decrease with downslope distance. Thermal theory relies on the increase in the mass of the current head through entrainment as the major mechanism for deceleration and, therefore, tends to underpredict the front velocity in the deceleration phase. **DOI: 10.1061/(ASCE) HY.1943-7900.0000500.** *© 2012 American Society of Civil Engineers.*

CE Database subject headings: Slopes; Thermal factors; Currents; Hydraulics.

Author keywords: Buoyancy-driven flows; Gravity currents; Sloping boundary; Thermal theory.

Introduction

Gravity currents, also known as density currents, are buoyancy-driven flows caused by a density difference. The density difference may be due to dissolved or suspended materials and temperature differentials. Gravity currents on slopes are commonly encountered in geophysical environments, for example, powder-snow avalanches and turbidity currents off the continental shelf, but they are also of interest in engineering applications mostly related to industrial safety and environmental protection. Readers are referred to Allen (1985), Fannelop (1994), and Simpson (1997) for more details about gravity currents and their relevance in natural science and engineering applications.

The interest in gravity currents has initiated a substantial amount of research using theoretical, experimental, and numerical methods. Much work has focused on gravity currents produced by instantaneous, finite buoyancy on a horizontal boundary, that is, lock-exchange flows (Benjamin 1968; Huppert and Simpson 1980; Marino et al. 2005; Huppert 2006). For gravity currents on a slope, the buoyancy source may be continuously maintained (Britter and Linden 1980; Parker et al. 1986) or released instantaneously with finite buoyancy (Beghin et al. 1981; Rastello and Hopfinger 2004). The focus here is on the gravity currents produced by a finite amount of buoyancy instantaneously released on a slope. Such gravity currents were experimentally studied and theoretically modeled with thermal theory in Beghin et al. (1981), which has formed the basis for many subsequent studies. For example, Dade et al. (1994) extended the theory to a gravity current on a slope with decreasing buoyancy because of particle settling; Rastello and Hopfinger (2004) studied a case in which the buoyancy increases as a result of resuspension of sediment. Apart from classic thermal theory, Webber et al. (1993), Tickle (1996), and Ross et al. (2002) alternatively used a shallow water model for an instantaneous release of buoyancy on a uniform slope. Birman et al. (2007) numerically investigated Boussinesq and non-Boussinesq gravity currents on sloping boundaries using two-dimensional simulations and found agreement with experiments designed to minimize three-dimensional dynamics. However, here it is shown that a three-dimensional configuration is warranted to accurately capture the different phases of gravity current motion, and the use of two-dimensional simulations is limited (Cantero et al. 2007).

The thermal theory developed by Beghin et al. (1981) for gravity currents follows the spirit of the famous Morton et al. (1956) in that the total released buoyancy is assumed to be contained in the gravity current head, into which the ambient fluid is entrained. The gravity current head was assumed to have a self-similar, semielliptical shape as it moves downslope. The acceleration and deceleration phases of gravity current on a slope were qualitatively described by thermal theory, and in particular, the height and length of the current head were predicted to increase linearly with downslope distance.

Recently, Maxworthy and Nokes (2007) reexamined the gravity current produced by an instantaneous bouyancy source that is composed of a slender body of dense fluid, where the lock length is twice as long as the lock height. It was found in such a case that the gravity current head does not contain the total released

[1]Dept. of Water Resources and Environmental Engineering, Tamkang Univ., Taiwan (corresponding author). E-mail: hdai@mail.tku.edu.tw

[2]Dept. of Civil and Environmental Engineering, Univ. of Delaware, Newark, DE 19716.

[3]National Council for Scientific and Technological Research, Bariloche Atomic Center, Bustillo 9500, San Carlos de Bariloche, Rio Negro, Argentina; Institute Balseiro, National Univ. of Cuyo—National Commission of Atomic Energy, Bustillo 9500, San Carlos de Bariloche, Rio Negro, Argentina.

[4]Dept. of Mechanical and Aerospace Engineering, University of Florida, Gainesville, FL 32611.

buoyancy when the current head forms; instead, it is continuously fed by the tail current from initiation until the maximum front velocity is reached. Therefore, the buoyancy in the head increases as the gravity current propagates downstream, similar to the gravity current on a slope produced by a continuous source (Britter and Linden 1980). Maxworthy and Nokes (2007) predicted that if lock length had been in the range 0.6–1.2 times lock height, the current head could have contained most of the dense fluid. For the buoyancy source in Beghin et al. (1981), in which the lock length-to-height ratio was 1.25, classic thermal theory was deemed principally adequate. However, whether the characteristics of the gravity current head are adequately described by, and whether appropriate assumptions are invoked by, thermal theory in the acceleration and deceleration phases in the configuration of Beghin et al. (1981) remain unknown and motivate our further investigation.

In this study, the problem of Beghin et al. (1981) is reinvestigated using direct numerical simulations (DNSs) of gravity currents, in which all scales of motion are fully resolved in space and time. The characteristics of gravity current on a slope, including height, length, and velocity of the head, can all be derived from the DNS results and compared with the experimental data and thermal theory given in Beghin et al. (1981). Also carefully reexamined here are the assumptions and predictions based on thermal theory.

Governing Equations and Numerical Formulation

Fig. 1 illustrates the gravity current configuration employed in the present work. The heavy fluid of density $\tilde{\rho}_1$ is confined to the shaded region and separated from the light fluid of density $\tilde{\rho}_0$. Here it is assumed that the density difference is small enough that the Boussinesq approximations can be adopted. The Boussinesq equations, where density variations are neglected in the inertia term and retained only in the buoyancy term, take the dimensionless form

$$\frac{\partial u_k}{\partial x_k} = 0, \tag{1}$$

$$\frac{\partial u_i}{\partial t} + \frac{\partial (u_i u_k)}{\partial x_k} = \rho e_i^g - \frac{\partial p}{\partial x_i} + \frac{1}{\mathrm{Re}} \frac{\partial^2 u_i}{\partial x_k \partial x_k}, \tag{2}$$

Fig. 1. Sketch of the quantities used in the formulation and thermal theory; the gravity current travels in the downslope direction, x_1, in a semielliptical form; spanwise direction, x_2, is pointing into the $x_1 x_3$ plane and follows the right-hand rule; H and L are the height and length of the gravity current head; x_0 is the distance measured from the virtual origin to the initial state; x is measured from the virtual origin to the center of mass of the gravity current head; x_f is measured from the virtual origin to the gravity current front; the initial buoyancy was confined in a lock of $l_0 \times h_0 = 0.4 \times 0.32$; all lengths are normalized by the channel half-height $\tilde{h}$; the computational domain is chosen as $L_{x_1} \times L_{x_2} \times L_{x_3} = 16 \times 3 \times 2$ for unhindered development of acceleration and deceleration phases; the gravity in direction $\tilde{e}_i^g$ makes an angle θ with the wall-normal direction x_3

$$\frac{\partial \rho}{\partial t} + \frac{\partial (\rho u_k)}{\partial x_k} = \frac{1}{\mathrm{ReSc}} \frac{\partial^2 \rho}{\partial x_k \partial x_k}. \tag{3}$$

Here u_i denotes the velocity vector, ρ the density, e_i^g the unit vector pointing in the gravity direction, and p the pressure. In the present study the channel considered is inclined at an angle θ; therefore, $e_i^g = (\sin\theta, 0, -\cos\theta)^T$. Furthermore, this paper focuses on $\theta = 10°$ to allow comparison with the work of Beghin et al. (1981). The variables in (1)–(3) are made dimensionless by channel half-height, $\tilde{h}$, as the length scale and buoyancy velocity, $\tilde{u}_b = \sqrt{\tilde{g}' \tilde{h}}$, as the velocity scale, where reduced gravity $\tilde{g}'$ is

$$\tilde{g}' = \tilde{g} \frac{\tilde{\rho}_1 - \tilde{\rho}_0}{\tilde{\rho}_0}. \tag{4}$$

The dimensionless pressure and density are given by

$$p = \frac{\tilde{p}}{\tilde{\rho}_0 \tilde{u}_b^2}, \qquad \rho = \frac{\tilde{\rho} - \tilde{\rho}_0}{\tilde{\rho}_1 - \tilde{\rho}_0}. \tag{5}$$

The Reynolds (Re) and Schmidt (Sc) numbers arise from the nondimensionalization of the equations and are defined by

$$\mathrm{Re} = \frac{\tilde{u}_b \tilde{h}}{\tilde{\nu}}, \qquad \mathrm{Sc} = \frac{\tilde{\nu}}{\tilde{\kappa}}, \tag{6}$$

where $\tilde{\nu}$ represents the kinematic viscosity, and $\tilde{\kappa}$ the diffusivity of the density field. Based on the observation that the influence of Schmidt number on flow is weak, Sc = 1 was employed in all simulations (Hartel et al. 2000; Bonometti and Balachandar 2008).

Note that (1)–(3) are made dimensionless by the length and velocity scales that are known a priori. It is equally customary in gravity current studies to define the front Reynolds number based on the actual front velocity, $\tilde{u}_f$, and current thickness, $\tilde{h}_f$, as

$$\mathrm{Re}_f = \frac{\tilde{u}_f \tilde{h}_f}{\tilde{\nu}}, \qquad \text{i.e., } \mathrm{Re}_f = u_f h_f \mathrm{Re}, \tag{7}$$

where dimensionless front velocity, u_f, and current thickness, h_f, are derived from the simulation results.

In the present investigation, the code described in Cortese and Balachandar (1995) based on the de-aliased pseudospectral method (Canuto et al. 1988) is employed, and a detailed validation of the code for lock-exchange flows is documented in Cantero et al. (2006, 2007). The governing equations are solved in the rectangular domain $L_{x_1} \times L_{x_2} \times L_{x_3}$ with resolution $N_{x_1} \times N_{x_2} \times N_{x_3}$. The width of the channel was chosen to be $L_{x_2} = 3$, which is sufficient for spanwise variation including several lobe and cleft structures (Hartel et al. 2000). The channel length in the streamwise direction was chosen to be $L_{x_1} = 16$ to allow full development of acceleration and deceleration phases and comparison with Beghin et al. (1981). If the effect of sidewalls can be neglected (Hartel et al. 2000; Cantero et al. 2006, 2007), in the streamwise and spanwise directions, periodic boundary conditions are employed as in

$$f(x_1, x_2, x_3, t) = \sum_{k_1, k_2} \hat{f}_{k_1, k_2}(x_3, t) e^{i2\pi k_1 x_1 / L_{x_1}} e^{i2\pi k_2 x_2 / L_{x_2}}, \tag{8}$$

where f represents the discretized variables, namely, velocity components, pressure, and density; and $\hat{f}$ represents the coefficients of Fourier transforms. The wavenumbers in the x_1 and x_2 directions are k_1 and k_2, respectively, which satisfy

$$|k_1| \leq \frac{N_{x_1}}{2}, \qquad |k_2| \leq \frac{N_{x_2}}{2}. \tag{9}$$

In the wall-normal direction, the Chebyshev expansion for $\hat{f}$ with Gauss–Lobatto quadrature points is employed, which provides higher resolution near the walls and allows straightforward treatment of boundary conditions. At the top and bottom boundaries, $x_3 = \pm 1$; the no-slip and no-flux conditions are employed for the velocity and density fields, that is,

$$u_i = 0, \qquad \frac{\partial \rho}{\partial x_3} = 0 \quad \text{at } x_3 = \pm 1. \qquad (10)$$

To solve the equations in the velocity–pressure formulation, the diffusion terms are treated implicitly using the Crank–Nicolson scheme. The convection and buoyancy-forcing terms are treated explicitly using the low-storage third-order Runge–Kutta scheme (Williamson 1980). The Arakawa method (Durran 1999), in which the convective and divergence forms of the nonlinear term are alternately used, is also employed for the convection term to reduce the aliasing error. In all simulations, the velocity field was initialized with fluid at rest; that is, $u_i = 0$ everywhere. The initial density field is prescribed constant values in the heavy and light fluid regions following the configuration of Beghin et al. (1981), with a steep error function-type transition between the two values (Hartel et al. 1997). The initial density field is also seeded with a minute random disturbance to ensure transition to turbulence (Cantero et al. 2006). In this paper are presented three-dimensional DNSs at four Reynolds numbers ($Re = 3 \times 10^3$, 5×10^3, 10^4, 2×10^4). To fully resolve the largest and smallest scales of gravity current motion in the computational domain ($L_{x_1} \times L_{x_2} \times L_{x_3} = 16 \times 3 \times 2$), the numerical meshes $N_{x_1} \times N_{x_2} \times N_{x_3} = 440 \times 84 \times 120$, $480 \times 96 \times 144$, $560 \times 128 \times 220$, and $880 \times 168 \times 330$ were selected for $Re = 3 \times 10^3$, 5×10^3, 10^4, and 2×10^4, respectively. The numerical meshes were chosen such that higher resolution is provided compared with reported channel flow (Moser et al. 1999) and gravity current (Cantero et al. 2006, 2007) simulations. The time step was chosen to produce a Courant number less than 0.5.

Thermal Theory Revisited

The flow configuration shown in Fig. 1 is again considered here. The intent is to make a comparison between DNS results and thermal theory. In this section, the theoretical treatment of Beghin et al. (1981) is summarized, and the bottom friction for the gravity currents on a slope is included. The gravity current head was assumed to have a semielliptical shape, which has a constant height-to-length aspect ratio $\kappa = H/L$. The density difference was assumed small enough so that the Boussinesq approximations hold; that is, $(\tilde{\rho}_1 - \tilde{\rho}_0)/\tilde{\rho}_0 \ll 1$, where $\tilde{\rho}_1$ and $\tilde{\rho}_0$ are the heavy and light fluid densities. Following the same normalization defined previously, the rate of change in linear momentum of the gravity current takes the dimensionless form

$$\frac{d(1 + \kappa_v) S_1 H L U}{dt} = B \sin\theta - C_f U^2 L, \qquad (11)$$

where H and L are dimensionless height and length of the semielliptical gravity current head. The dimensionless buoyancy contained in the current head, $B = \rho H L S_1$, is the driving force for the head and was assumed an invariant equal to the total released buoyancy in uniform surroundings. The bottom friction force is proportional to the length of the head, where $C_f \approx 10^{-2}$ is the friction coefficient (Rastello and Hopfinger 2004). The shape factor $S_1 = \pi/4$ denotes the ratio of the cross-sectional area to the product HL, and $\kappa_v = 2\kappa$ is the added mass coefficient for a semiellipse. Note here that the dimensionless buoyancy, B, can be regarded

as the product of the mixed fluid contained in the head, HLS_1, and the averaged density within the head, ρ. Before the lock gate is released, $\rho = 1$ and the amount of heavy fluid is $l_0 h_0$; therefore, $B = l_0 h_0$ at $t = 0$. When the gravity current head develops on a slope after the gate is released, the size of the current head increases while the averaged density within the head decreases. It was assumed in thermal theory that the size of head and averaged density varied in such a way that the buoyancy in the head was unchanged and equal to the total buoyancy during the course of gravity current motion; that is, $B = l_0 h_0$ for all time. Later, this assumption is clarified in more detail. The center of mass velocity of the gravity current head is denoted by U. The conservation of mass is given by the dimensionless form

$$\frac{d(S_1 HL)}{dt} = S_2 (HL)^{1/2} \alpha U, \qquad (12)$$

where the other shape factor $S_2 = (\pi/2^{3/2})(4\kappa^2 + 1)^{1/2}/\kappa^{1/2}$ indicates the ratio of the circumference to $\sqrt{HL}$ for a semiellipse; and α is the entrainment coefficient, which is a function of slope angle only. Eqs. (11) and (12) allow the analytical solution

$$H = \frac{1}{2}\frac{S_2}{S_1}\kappa^{1/2}\alpha x, \qquad L = \frac{1}{2}\frac{S_2}{S_1}\kappa^{-1/2}\alpha x \qquad (13)$$

where x is the dimensionless distance measured from the virtual origin defined by $H = L = 0$ (Beghin et al. 1981). Taking advantage of the symmetry property of the semielliptical shape, the distance from the virtual origin to the gravity current front location x_f is given by

$$x_f = \left(1 + \frac{1}{4\sqrt{\kappa}}\frac{S_2}{S_1}\alpha\right)x \qquad (14)$$

When the gravity current is initialized with heavy fluid at rest, as considered here, the center of mass velocity takes the form

$$U = C\left[\frac{x_0}{x} - \left(\frac{x_0}{x}\right)^{4 + \frac{4C_f}{\alpha S_2(1 + \kappa_v)\sqrt{\kappa}}}\right]^{1/2} \quad \text{and}$$

$$C = \left[\frac{8 S_1 B \sin\theta}{3(1 + \kappa_v)\alpha^2 S_2^2 + 4C_f \alpha S_2 \kappa^{-1/2}}\frac{1}{x_0}\right]^{1/2} \qquad (15)$$

where x_0 denotes the dimensionless distance from the virtual origin to the center of mass at the initial state of the motion. In practice, the location of virtual origin and consequently x_0 are not known a priori. However, when the gravity current head forms and develops on a slope, the acceleration phase in which the height and length of the current head grow linearly with downslope distance, also known as the initial similarity state in Beghin et al. (1981), can be identified. Therefore, it is possible to extrapolate the linear relationship between the height and length of the current head and downslope distance to identify the virtual origin and, consequently, x_0 and x_f. The gravity current front velocity is then given by

$$U_f = U\left(1 + \frac{1}{4\sqrt{\kappa}}\frac{S_2}{S_1}\alpha\right), \qquad (16)$$

where the maximum front velocity is $U_{f,\text{max}} \approx 0.687C[1 + S_2\alpha/(4S_1\sqrt{\kappa})]$ when $C_f \to 0$.

Beghin et al. (1981) conducted a series of gravity current experiments produced from an instantaneous buoyancy source on inclined boundaries in the range between 5° and 90°. In particular, the velocity of gravity current head on a 10° slope was presented therein. Following the normalization in the previous section, the heavy fluid was confined in a lock of $l_0 \times h_0 = 0.4 \times 0.32$, as indicated in Fig. 1; the Reynolds number was approximately 5×10^4

in their experiments. For such a gravity current on a 10° slope, it was reported that $H = 0.07x_f$ and $L = 0.32x_f$; that is, $\kappa = 0.28$ and $\alpha = 0.1$.

Results

The features obtained from DNS results are described next in the light of thermal theory. All simulations were continued until both acceleration and deceleration phases were fully developed.

Flow Characteristics

As the gravity current travels down a slope, it entrains and mixes with ambient fluid. Therefore, gravity current grows while its density decreases. For easy visualization of the gravity current and an unambiguous measure of buoyancy, width-averged density, $\bar{\rho}$, and equivalent height, $\bar{h}$, are defined as

$$\bar{\rho}(x_1, x_3, t) = \frac{1}{L_{x_2}} \int_0^{L_{x_2}} \rho(x_1, x_2, x_3, t)dx_2,$$

$$\bar{h}(x_1, t) = \int_{-1}^{1} \bar{\rho}(x_1, x_3, t)dx_3 \tag{17}$$

respectively (Shin et al. 2004). To illustrate the concept of equivalent height, in fluid columns filled entirely by the light ambient fluid, the equivalent height is zero; in fluid columns filled entirely by the released heavy fluid, the equivalent height is L_{x_3}. According to the configuration as shown in Fig. 1, the total released buoyancy in the channel is given by

$$\int_0^{L_{x_3}} \bar{h}(x_1, t)dx_1 = l_0 \times h_0 \quad \forall \, t \tag{18}$$

Evolutions of the width-averaged density field at Re $= 10^4$ and equivalent height for gravity currents at three other Reynolds numbers are shown in Figs. 2 and 3. Note that the size of the gravity
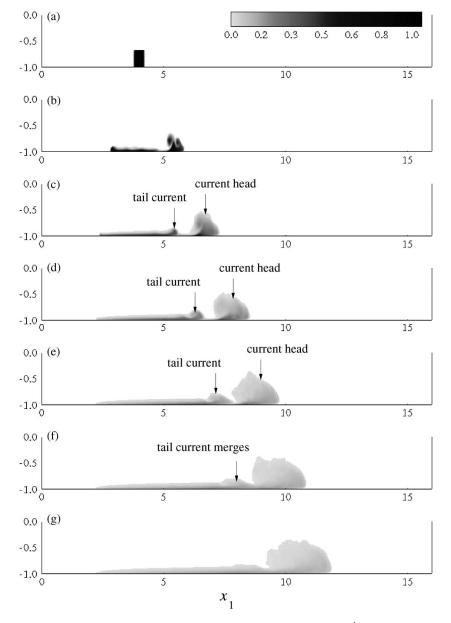

Fig. 2. Gravity current produced from an instantaneous buoyancy source on a 10° slope at Re $= 10^4$; the current is visualized with width-averaged density contours; six different times with initial conditions are shown; the time interval between consecutive frames is 5 dimensionless time units; x_1 denotes the streamwise direction and only the bottom half of the channel is shown ($-1 \leq x_3 \leq 0$)
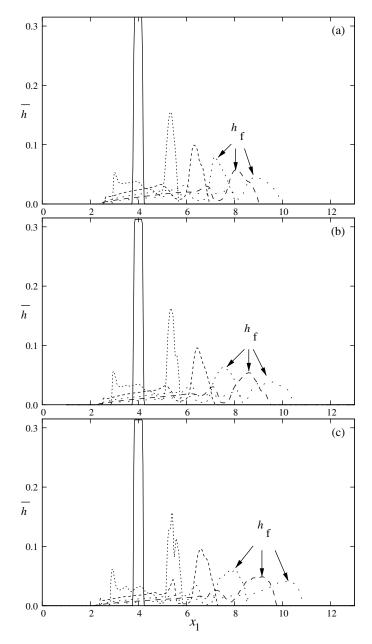
Fig. 3. Evolution of the gravity current on a 10° slope at different Reynolds numbers visualized by the equivalent height defined by Eq. (17): (a) $\mathrm{Re} = 3 \times 10^3$, (b) $\mathrm{Re} = 5 \times 10^3$, (c), $\mathrm{Re} = 10^4$; in each panel, the time interval between consecutive instances is 5 dimensionless time units; arrows indicate the local maximum in equivalent height, h_f, as the gravity current thickness in the definition of front Reynolds number, Eq. (7)

current head increases as the gravity current moves downslope, whereas the equivalent height decreases during the course of motion, because of both mixing and spreading on the slope. Following the release of initial buoyancy, the semielliptical head contains only part of the total released buoyancy; the remaining part forms a separated tail current that joins the head at a later stage, as shown in Fig. 2.

Of particular interest here is the growth of the size of the gravity current head, as it gives a direct measure and comparison with thermal theory. Based on Fig. 2 it is not unreasonable to approximate the gravity current head with a semielliptical shape. To define the

length and height of the semielliptical head, here advantage is taken of the equivalent height defined by (17) in that the semielliptical head represented by a local maximum in equivalent height, h_f, which is indicated in Fig. 3, is separated from the tail current by a local minimum in equivalent height. This local maximum, h_f, designated as the gravity current thickness in the definition of front Reynolds number, along with the local minimum in equivalent height, can be unambiguously identified. The front of the current is taken to be at the location given by $\bar{h} = 0.001$, and because of the sharpness of the density gradient here, the location of the front is insensitive to the actual value of $\bar{h}$ chosen to identify it. The length of the semielliptical head, L, is defined as the distance between current front and the local minimum in equivalent height. The height of the semielliptical head, H, is defined as the distance between the bottom boundary and gravity current edge chosen to be $\bar{\rho} = 0.1$ at the streamwise location where h_f is identified. If there were no mixing, H would be equal to the current thickness, h_f. Because of mixing, the density within the head is not uniform; consequently, H is generally greater than h_f. As illustrated in Fig. 4(a), the choice of $\bar{\rho}$ used here to identify the head height was made to quantify observations of the growth in height, $H \sim 0.07x_f$, consistently with the reported experimental observation. The virtual origins, followed by x_0 and x_f, are then identified through an extrapolation procedure given in Beghin et al. (1981). However, note that the location of the virtual origin based on extrapolating head height differs from that based on extrapolating head length. To consistently show the growth patterns of height and length of the gravity current head, x_f is measured from the virtual origin, and the lines separating acceleration and deceleration phases may look different in the plots showing the growth in height and length with distance. During the initial stage of gravity current motion, the height and length of the gravity current head increase linearly with downslope distance, as predicted by Eq. (13) and shown in Fig. 4. However, Fig. 4 also illustrates that the height and length of the current head do not follow a linear relationship with downslope distance throughout the entire course of motion. This linear relationship between head size and downslope distance, Eq. (13), is strictly observed only at the initial stage of the gravity current motion.

As will be explained in more detail, the gravity current on a slope goes through the acceleration and deceleration phases. In the acceleration phase, after the gravity current head is formed, the height and length of the current head grow linearly with downslope distance, which is in agreement with thermal theory. In the deceleration phase, however, the height and length on average grow more slowly with downslope distance as compared with the acceleration phase. Furthermore, the semielliptical head experiences multiple sporadic reductions in its height as indicated in Fig. 4(b) by the arrows for the $\mathrm{Re} = 10^4$ case. The relationship reported by Beghin et al. (1981) for head height, $H = 0.07x_f$, and head length, $L = 0.32x_f$, appears to be appropriate in the acceleration phase, but not in the deceleration phase, of gravity current motion. In Fig. 5, aspect ratio, κ, is plotted against downslope distance. Following Morton et al. (1956), the assumption of self-similarity requires the aspect ratio to be a constant. It might be reasonable to adopt a constant aspect ratio for the acceleration phase; however, the aspect ratio in the deceleration phase decreases with downslope distance. Note that in Morton et al. (1956), the good reason to assume a constant aspect ratio was that the freely rising buoyant cloud was laterally unconfined. But for gravity currents on a slope, the presence of the bottom boundary makes the self-similarity assumption less appropriate. It is also observed in Figs. 4 and 5 that as Reynolds number increases, the height and aspect ratio of the current head decrease. The dependence on Reynolds number suggests that
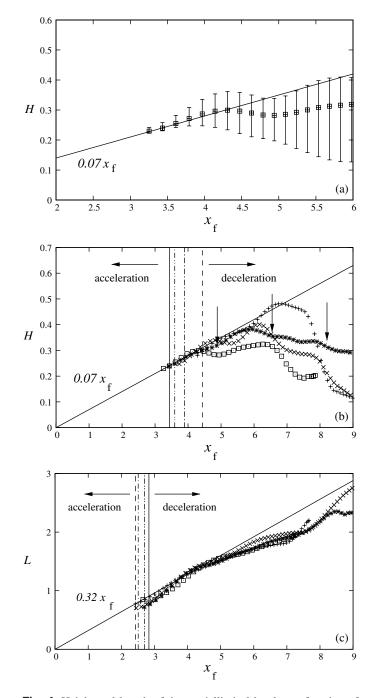
Fig. 4. Height and length of the semielliptical head as a function of distance from the virtual origin to the front: (a) H versus x_f for $Re = 2 \times 10^4$; head height ($\square$) is quantified based on the choice of $\bar{\rho} = 0.1$; upper and lower bounds indicate the height based on the choices of $\bar{\rho} = 0.01$ and $\bar{\rho} = 0.2$, respectively. (b) H versus x_f. (c) L versus x_f. In (b) and (c), symbols represent DNS results: +, $Re = 3 \times 10^3$; ×, $Re = 5 \times 10^3$; *, $Re = 10^4$; $\square$, $Re = 2 \times 10^4$. Solid lines, $H = 0.07x_f$ and $L = 0.32x_f$, represent experimental observations reported Beghin et al. (1981); dashed lines denote the locations at the end of the acceleration phase of each Reynolds number: ––, $Re = 3 \times 10^3$; –.–, $Re = 5 \times 10^3$; –..–, $Re = 10^4$; –…–, $Re = 2 \times 10^4$; arrows in (b) indicate instances where the height of the head decreases for the case $Re = 10^4$

the mechanism of vortex rollup and breakdown at the current interface will work vigorously when the gravity current interface is turbulent.

Front Velocity

Front velocity, u_f, can be obtained from the time dependence of the front location, x_f as

$$u_f = \frac{dx_f}{dt}. \qquad (19)$$

In Fig. 6(a), front velocity is plotted against downslope distance as a function of Reynolds number. Both the acceleration and deceleration phases are successfully captured in accord with the experimental data ($\diamond$); maximum velocity is reached at the end of the acceleration phase followed by deceleration of the gravity current. According to Beghin et al. (1981), it is noted that the distinct jump in the experimental data at $x_f \approx 3.7$ is not physical, but merely an error associated with the finite-differencing process. Therefore, the maximum front velocity in the experimental data is taken as $u_f \approx 3.8$ derived from the acceleration phase. In Fig. 6(b), the front Reynolds number, defined by Eq. (7), is plotted against downslope distance. The maximum front velocities and the dependence on Reynolds number are illustrated in Fig. 6(c), with predictions with thermal theory based on different levels of buoyancy contained in the gravity current head. The lower velocities seen in the direct simulations are attributed to Reynolds number effects (Simpson and Britter 1979; Parsons and Garcia 1998; Hartel et al. 2000). On the basis of thermal theory, the more buoyancy that is contained in the head, the higher is the maximum front velocity that be reached. According to Beghin et al. (1981), the total released buoyancy was assumed to be contained in the head ($B = l_0 h_0$), and thermal theory showed reasonable agreement with the experimental data. However, as will be seen in Fig. 7(b), the amount of heavy fluid contained in the head at the end of the acceleration phase is in fact only a fraction of the total released heavy fluid.

In the deceleration phase, while overall front velocity decreases with downslope distance, instantaneous front velocity may not do so, as revealed both by the experimental data of Beghin et al. (1981) and the DNS results in the present work as indicated in Fig. 6(a). The arrows in Fig. 6(a) are at the same instants as in Fig. 4(b), where the height of the current head episodically decreased at $Re = 10^4$. Interestingly, following the reduction in height of the gravity current head, instantaneous front velocity decreases less
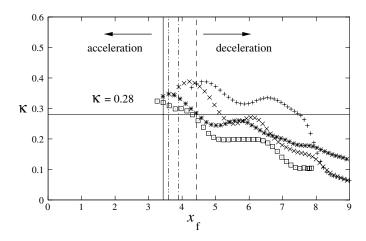

Fig. 5. Plot of ratio of the semielliptical head, $\kappa = H/L$, against distance from virtual origin to front location, x_f, symbols represent DNS results: +, $Re = 3 \times 10^3$; ×, $Re = 5 \times 10^3$; *, $Re = 10^4$; $\square$, $Re = 2 \times 10^4$; solid line denotes $\kappa = 0.28$ as reported in Beghin et al. (1981) for the gravity current on a 10° slope; dashed lines denote the same locations as in Fig. 4
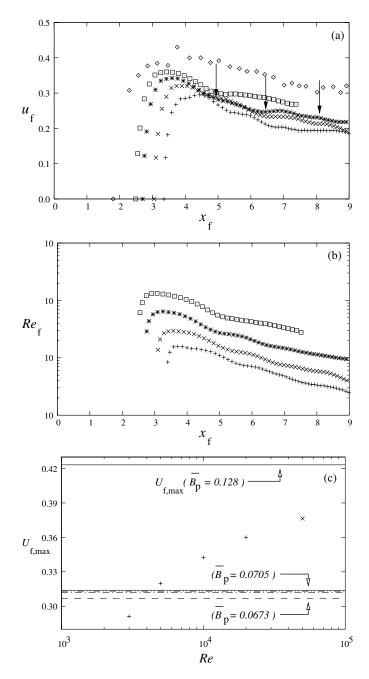
Fig. 6. Front velocity of the gravity current down a 10° slope: (a) Front velocity u_f versus distance from virtual origin to front location, x_f, as a function of Reynolds number; symbols represent DNS and experimental results: +, Re = 3×10^3 (DNS); ×, Re = 5×10^3 (DNS); *, Re = 10^4 (DNS), □, Re = 2×10^4 (DNS); ◇: Re = 5×10^4 [experimental data from Beghin et al. 1981]. (b) Front Reynolds number, Re$_f$ defined by Eq. (7), versus x_f [symbols as in (a)]. (c) Maximum front velocity $U_{f,\text{max}}$ versus Reynolds number: +, DNS; ×, experimental data; dashed and solid lines represent the maximum front velocity predictions of thermal theory` based on $\kappa = 0.28$, $\alpha = 0.1$, as reported in Beghin et al. (1981), and different levels of contained buoyancy in the head at the end of acceleration phase: $--$, $\bar{B}_p = 0.0673$; $-.-$, $\bar{B}_p = 0.0695$; $-..-$, $\bar{B}_p = 0.0701$; $-...-$, $\bar{B}_p = 0.0705$; $-$, $\bar{B}_p = 0.128$

rapidly or even increases in the deceleration phase. The episodic variation in height and speed of the current is due to vortex rollup and interaction at the interface between the current and the ambient fluid (Cantero et al. 2006), which can be explained in short as

follows: as the heavy fluid is advected by the vortices, the center of gravity of the head decreases periodically, which contributes to a reduction in the height of the head and an increase in the front velocity, because temporarily the lowering of center of gravity contributes to potential energy being converted to kinetic energy. This observation is more amplified in the two-dimensional simulations because the spanwise vortex structures are not allowed to break up (Cantero et al. 2006, 2007).

Buoyancy in the Head as an Invariant?

In classic thermal theory, it was assumed and generally perceived that the total released buoyancy was conserved in the gravity current head and, as such, treated as an invariant. To clarify this assumption, here effective buoyancy is defined as the integral of equivalent height within the gravity current head of length L, that is,

$$\bar{B}(t) = \int_L \bar{h}(x_1, t)dx_1, \qquad (20)$$

where subscript L in the integral denotes that the integration is performed only in the current head region. Note that if total buoyancy were to be conserved in the current head, effective buoyancy would be identical to the initial buoyancy released, that is, $\bar{B} = l_0 h_0$. Several mechanisms have been found to be responsible for nonconserving buoyancy in gravity current head on a slope. For example, the sediment can be entrained from the bed into the current and, therefore, increase total buoyancy (Parker et al. 1986; Rastello and Hopfinger 2004); the buoyancy in the gravity current can be continuously fed by tail current from behind the head from initiation (Maxworthy and Nokes 2007); deposition of fine sediment from the gravity current renders reduced buoyancy (Dade et al. 1994). Note that none of these mechanisms are directly applicable here. In Fig. 7(a), effective buoyancy is plotted against downslope distance, which reveals that as the buoyancy is released on a slope, only part of the total released buoyancy is contained in the gravity current head; moreover, the contained buoyancy is not conserved during the course of motion, either. It is also worth noting that the decreasing in buoyancy in the head is observed to diminish as Reynolds number increases.

As a verification, Eq. (18) is also evaluated to ensure that the total released buoyancy is conserved in the channel, as shown in Fig. 7(a) and required by the volume integral of Eq. (3). Note that when the gravity current head forms, the maximum buoyancy contained in the head is approximately 55–58% of the total released buoyancy. As the gravity current develops downslope, the contained buoyancy in the head decreases in the deceleration phase. In Fig. 7(b), the plot of effective buoyancy at the end of the acceleration phase, $\bar{B}_p$, against Reynolds number reveal that $\bar{B}_p$ slightly increases as Re increases. As observed in Figs. 7(a) and 7(b), the Reynolds number plays a role in the level of buoyancy contained in the head. As Reynolds number increases, more buoyancy is contained in and transported with the head downslope. The buoyancy in the head, therefore, is strictly not an invariant. Further downslope in the deceleration phase, the buoyancy in the head increases in the Re = 10^4 and Re = 2×10^4 cases because the tail current joins and recharges the head with buoyancy.

Comparisons with Two-Dimensional Simulation and with Free-Slip Wall Condition

Two-Dimensional Simulation
Although the computations reported in this study are three-dimensional, it is helpful to compare the results with the two-dimensional simulation and identify their differences. A
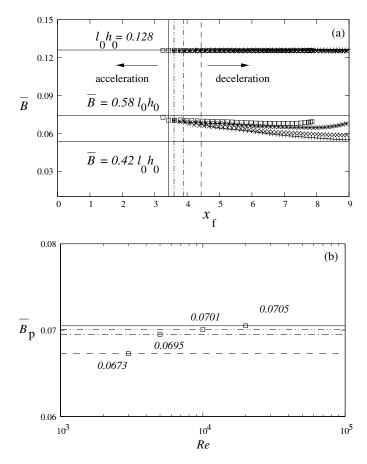
Fig. 7. Effective buoyancy contained in the gravity current head: (a) Effective buoyancy, $\bar{B}$ versus distance from virtual origin to front location, x_f, symbols represent DNS results: $+$, $Re = 3 \times 10^3$; $\times$, $Re = 5 \times 10^3$; $*$, $Re = 10^4$; $\square$, $Re = 2 \times 10^4$; effective buoyancy is in the range between $0.42l_0h_0$ and $0.58l_0h_0$ during the course of motion; buoyancy in the channel is also evaluated to ensure that the total released buoyancy is conserved total buoyancy in the channel is identical for the four cases and falls on $l_0 \times h_0 = 0.128$ as required; dashed lines denote the same locations as in Fig. 4. (b) Effective buoyancy at the end of the acceleration phase, $\bar{B}_p$, versus Reynolds number

two-dimensional simulation of $Re = 10^4$ was performed using $N_{x1} \times N_{x3} = 560 \times 220$ following the corresponding three-dimensional configuration. As shown in Fig. 8, except in the initial stage of acceleration, two-dimensional results underpredict front velocity compared with three-dimensional results at the same Reynolds number. Further downslope in the deceleration phase, two-dimensional results show pronounced oscillations in front velocity. These observations are in agreement with simulations of gravity current on a horizontal boundary (Cantero et al. 2006, 2007). Fig. 9 further shows the span-averaged spanwise vorticity with density contours. Note that interfacial vortices form and interact in the two-dimensional configuration [Fig. 9(c) and 9(d)], but the vortices are not persistent in the three-dimensional simulation at the same instants [Fig. 9(g) and 9(h)]. Linear stability analysis has also shown that these co-rotating vortices formed in gravity currents are unstable and will promptly break up into smaller structures (Dai and Garcia 2009). For the purpose of this study, it is therefore necessary to use three-dimensional simulations because of the artifical nature and limited representation of the gravity current motion by a two-dimensional configuration.
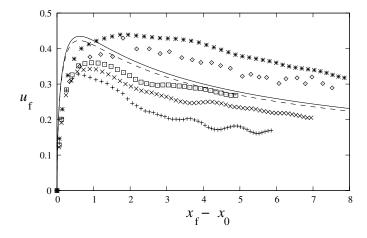

Fig. 8. Front velocity versus downslope distance in five illustrative cases with thermal theory predictions at large Reynolds numbers: $+$, two-dimensional simulation at $Re = 10^4$; $\times$, three-dimensional simulation at $Re = 10^4$; $\square$, three-dimensional simulation at $Re = 2 \times 10^4$; $\diamond$, experimental data at $Re = 5 \times 10^4$; $*$, three-dimensional simulation at $Re = 10^4$ with free-slip wall condition; solid and dashed lines represent the predictions based on thermal theory at large Reynolds number when $C_f = 0$ and $C_f = 0.01$, respectively

Influence of the No-Slip Wall Condition
In the reported simulations, the no-slip condition is imposed on the walls, whereas bottom friction was neglected in the original thermal theory (Beghin et al. 1981). To clarify the influence of the bottom boundary condition, we performed a simulation of $Re = 10^4$ following the same parameters in three-dimensional simulations, but chose a free-slip condition at the bottom wall. Fig. 8 also shows the front velocity of a gravity current on a free-slip wall. The free-slip front velocity appears to be significantly higher than the results under the no-slip condition and overpredicts the experimental data at an even higher Reynolds number. Although the bottom friction greatly alters the directly simulated gravity current velocity, the thermal theory prediction changes little with consideration of the drag term. The explanation for the difference in velocity reduction between simulations and theory is that thermal theory relies on the increase in fluid mass of the current head through the entrainment of ambient fluid as the major mechanism for deceleration. The direct influence of the drag coefficient, as compared with the effect of mass increase in the current head, is not significant. Not only does bottom friction in the simulations reduce front velocity through the direct influence of friction, but also the heavy fluid in the current head is sheared off along the bottom, which reduces the driving force and front velocity, indirectly and significantly. Also note that according to the DNS results, the gravity current head on a slope grows less rapidly or decreases in the deceleration phase than in the acceleration phase, as indicated in Fig. 4, and travels in a more "streamlined" front with decreasing aspect ratio. Therefore, the gravity current head in the deceleration phase actually contains less ambient fluid mass than predicted by thermal theory. Because of overestimation of the ambient fluid entrained into the head, thermal theory tends to underpredict front velocity in the deceleration phase.

Conclusion
This paper has presented three-dimensional DNS results of gravity currents on a slope and made a comparison with the classic thermal theory developed in Beghin et al. (1981).
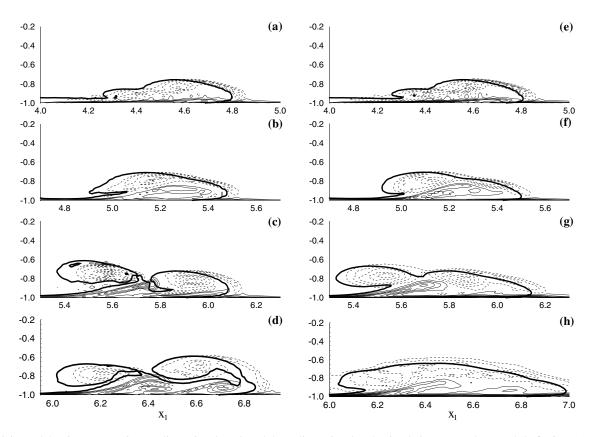
Fig. 9. Vorticity and density contours in two-dimensional (a–d) and three-dimensional (e–h) simulations at $t = 2$ (a, e), 4 (b, f), 6(c, g), and 9.5 (d, h) at $Re = 10^4$; thick solid lines represent the contours of $\rho = 0.1$; thin solid and dashed lines represent positive and negative span-averaged spanwise vorticity contours, respectively; vortex structures are persistent in two-dimensional simulation

It has been shown that maximum front velocity increases as Reynolds number increases. In the acceleration phase of gravity current motion, the size and velocity of gravity current increase, but the maximum buoyancy contained in the gravity current head is only part of the total released buoyancy; the level of buoyancy contained in the head during gravity current motion depends on Reynolds number. In the deceleration phase, sporadic reductions in the height of the current head occur, and therefore, the gravity current head decreases in size and buoyancy. In addition, in the deceleration phase, instantaneous front velocity may decrease less rapidly or even increase with downslope distance. This observation is identified in both the DNS results in this work and the experimental data of Beghin et al. (1981). Considering both the acceleration and deceleration phases of gravity current motion on a slope, the buoyancy contained in the gravity current is not an invariant, because the mixed fluid is shed from the head; in addition, buoyancy can be fed into the head at a later stage from the joining tail current.

Although thermal theory qualitatively indicates the acceleration and deceleration phases of gravity current traveling down a slope, it is worth recounting the main assumption made by Beghin et al. (1981). In thermal theory, it is assumed that the total released buoyancy is contained in the head for all time; therefore, the total buoyancy was conserved in the gravity current. Furthermore, the size of the gravity current, represented by the height and length of the semielliptical head, increases linearly with downslope distance. The current work has shown that only about 55–58% of the total buoyancy is contained in the gravity current head. In addition, it has also been shown that the height and aspect ratio of the head and the buoyancy contained within it may all decrease in the deceleration phase. Thermal theory relies on the increase in

the mass of the current head resulting from entrainment as the major mechanism for deceleration and, therefore, tends to underpredict front velocity in the deceleration phase. Note that the thermal theory for the gravity currents on a slope originates from Morton et al. (1956); however, although there was a good reason to adopt the self-similarity assumption for a laterally unconfined rising buoyant cloud (Morton et al. 1956), the presence of a bottom boundary in a gravity current case makes this assumption less appropriate.

The findings in this work suggest that classic thermal theory may need to be modified to allow more accurate description of the gravity current on a slope. Toward this goal, further investigations are underway.

Acknowledgments

References

Allen, J. (1985). *Principles of Physical Sedimentology*, Allen & Unwin, London.

Beghin, P., Hopfinger, E. J., and Britter, R. E. (1981). "Gravitational convection from instantaneous sources on inclined boundaries." *J. Fluid Mech.*, 107, 407–422.

Benjamin, T. B. (1968). "Gravity currents and related phenomena." *J. Fluid Mech.*, 31(02), 209–248.

Birman, V. K., Battandier, B. A., Meiburg, E., and Linden, P. F. (2007). "Lock-exchange flows in sloping channels." *J. Fluid Mech.*, 577, 53–77.

Bonometti, T., and Balachandar, S. (2008). "Effect of Schmidt number on the structure and propagation of density currents." *Theor. Comput. Fluid Dyn.*, 22(5), 341–361.

Britter, R. E., and Linden, P. F. (1980). "The motion of the front of a gravity current travelling down an incline." *J. Fluid Mech.*, 99, 531–543.

Cantero, M., Balachandar, S., Garcia, M., and Ferry, J. (2006). "Direct numerical simulations of planar and cylindrical density currents." *J. Appl. Mech.*, 73(6), 923–930.

Cantero, M., Lee, J., Balachandar, S., and Garcia, M. (2007). "On the front velocity of gravity currents." *J. Fluid Mech.*, 586, 1–39.

Canuto, C., Hussaini, M., Quarteroni, A., and Zang, T. (1988). *Spectral Methods in Fluid Dynamics*, Springer, Berlin.

Cortese, T., and Balachandar, S. (1995). "High performance spectral simulation of turbulent flows in massively parallel machines with distributed memory." *Int. J. Supercomputer Appl.*, 9(3), 187–204.

Dade, W. B., Lister, J. R., and Huppert, H. E. (1994). "Fine-sediment deposition from gravity surges on uniform slopes." *J. Sediment. Res.*, 64, 423–432.

Dai, A., and Garcia, M. (2009). "Stability of a pair of counter-rotating and co-rotating vortices of different strengths." *J. Eng. Mech.*, 135(6), 591–595.

Durran, D. (1999). *Numerical Methods for Wave Equations in Geophysical Fluid Dynamics*, Springer, Berlin.

Fannelop, T. K. (1994). *Fluid Mechanics for Industrial Safety and Environmental Protection*, Elsevier, Amsterdam.

Hartel, C., Meiburg, E., and Necker, F. (2000). "Analysis and direct numerical simulation of the flow at a gravity-current head. Part 1. Flow topology and front speed for slip and no-slip boundaries." *J. Fluid Mech.*, 418, 189–212.

Hartel, C., Michaud, L. K. M., and Stein, C. (1997). "A direct numerical simulation approach to the study of intrusion fronts." *J. Eng. Math.*, 32(2–3), 103–120.

Huppert, H. (2006). "Gravity currents: A personal perspective." *J. Fluid Mech.*, 554, 299–322.

Huppert, H., and Simpson, J. (1980). "The slumping of gravity currents." *J. Fluid Mech.*, 99, 785–799.

Marino, B., Thomas, L., and Linden, P. (2005). "The front condition for gravity currents." *J. Fluid Mech.*, 536, 49–78.

Maxworthy, T., and Nokes, R. I. (2007). "Experiments on gravity currents propagating down slopes. Part 1. The release of a fixed volume of heavy fluid from an enclosed lock into an open channel." *J. Fluid Mech.*, 584, 433–453.

Morton, B. R., Taylor, G. I., and Turner, J. S. (1956). "Turbulent gravitational convection from maintained and instantaneous sources." *Proc. R. Soc. A*, 234(1196), 1–23.

Moser, R. D., Kim, J., and Mansour, N. N. (1999). "Direct numerical simulation of turbulent channel flow up to $Re_\tau = 590$." *Phys. Fluids*, 11(4), 943–945.

Parker, G., Fukushima, Y., and Pantin, H. (1986). "Self-accelerating turbidity currents." *J. Fluid Mech.*, 171, 145–181.

Parsons, J. D., and Garcia, M. H. (1998). "Similarity of gravity current fronts." *Phys. Fluids*, 10(12), 3209–3213.

Rastello, M., and Hopfinger, E. J. (2004). "Sediment-entraining suspension clouds: A model of powder-snow avalanches." *J. Fluid Mech.*, 509, 181–206.

Ross, A. N., Linden, P. F., and Dalziel, S. B. (2002). "A study of three-dimensional gravity currents on a uniform slope." *J. Fluid Mech.*, 453, 239–261.

Shin, J., Dalziel, S., and Linden, P. (2004). "Gravity currents produced by lock exchange." *J. Fluid Mech.*, 521, 1–34.

Simpson, J. (1997). *Gravity Currents*, 2nd Ed., Cambridge Univ. Press, London.

Simpson, J. E., and Britter, R. E. (1979). "The dynamics of the head of a gravity current advancing over a horizontal surface." *J. Fluid Mech.*, 94(3), 477–495.

Tickle, G. (1996). "A model of the motion and dilution of a heavy gas cloud released on a uniform slope in calm conditions." *J. Hazard. Mater.*, 49(1), 29–47.

Webber, D., Jones, S., and Martin, D. (1993). "A model of the motion of a heavy gas cloud released on a uniform slope." *J. Hazard. Mater.*, 33, 101–122, ⟨http://dx.doi.org/10.1016/0304-3894(93)85066-N⟩.

Williamson, J. H. (1980). "Low-storage Runge–Kutta schemes." *J. Comput. Phys.*, 35(1), 48–56.